TB13

19th International Symposium of Ballistics, 7–11 May 2001, Interlaken, Switzerland

ON THE BEHAVIOUR OF LONG-ROD PENETRATORS UNDERGOING LATERAL ACCELERATIONS

H. F. Lehr[1] – E. Wollmann[1] – W. Lanz[2] – K. Sterzelmeier[1]

[1] French-German Research Institute of Saint-Louis (ISL), Postfach 1260, 79574 Weil am Rhein, Germany
[2] Swiss Ordnance Enterprise Corp., Allmendstrasse 86, 3602 Thun, Switzerland

Experiments with long-rod penetrators of very high aspect ratios demonstrate that these slender cylinders can fail because of severe structural integrity and stability problems during acceleration and flight phase. In a previous paper the authors gave some hints in order to solve that problem. If lateral accelerations were looked at as reason for the bending of the rods a new parameter could be defined standing for a constant stress level for penetrators of various dimensions. The parameter itself is a simple combination of purely geometric main measures of the rod, i.e. diameter and length. It will be shown that the parameter serves as an advantageous tool while designing long-rod penetrators; it is also a well suited means to identify bending stresses from experimental penetrator profiles and to compare experiments of different scale to each other. Stresses are calculated from the maximum deflection of bended rods from both model and real-scale experiments. Furthermore experiments at constant acceleration demonstrate higher stresses for penetrators with constant aspect ratios but increasing geometric dimensions of the rods.

INTRODUCTION

The requirement of a steadily increasing perforation power and the need to defeat different target types have resulted in quite sophisticated kinetic-energy long-rod penetrators. Because of the limited energy available and the physical parameters ruling the perforation power, i.e. density and length of the projectile as well as striking velocity, these rods show relatively high aspect ratios.

As a protection measure against this threat a number of targets are known with the intention to break these slender cylinders into pieces (e.g. active or reactive protection). This is of course a very effective method to defeat the penetrator as these slender rods quite often fail because of severe structural integrity and stability problems during the acceleration and flight phase and even more during penetration if strained by lateral forces. Thus it seems useful to discuss possibilities of hardening the long-rod projectile against

this threat of transverse forces and to examine the consequences for the design of penetrators as well as conclusions that can be drawn from specific experiments.

BENDING OF LONG-ROD PENETRATORS

As well known, long-rod penetrators often show stability and integrity problems during acceleration; flight phase and target interaction. Model-scale experi-ments with subcalibre projectiles made of tungsten heavy metal with diameters of 6 mm and aspect ratios of 40 (Figure 1) demonstrate these effects. As an example a flexure of the penetrator at 1.5 m off the muzzle is clearly visible in Figure 2a (upper part); another experiment with a strong flexure in the later flight phase is shown in Figure 2b.

Stability problems such as buckling, bending or bending vibrations are all the more likely as the fineness ratio of the projectile is high [1, 2]. This will possibly result in a loss of efficiency or even fracture of the projectile. During the target interaction process – and even more evident during the penetration of targets which exercise a transverse load on the rod – these projectiles bear extreme loads. Two examples of such projectile-target interactions are shown in Figure 4 with a bended penetrator and broken one, respectively.

The characteristic measures usually taken to define rod penetrators are mass, length and diameter as well as the fineness ratio. This quantity, i.e. the L/D-quotient, is the determining projectile shape factor and is commonly used as a group parameter in descriptions and diagrams. Certainly, the aspect ratio is a suitable reference parameter for the comparison of scaled and full-scale experiments or while applying scaling laws or special transformation rules for penetrators with constant *L/D*-ratios [3], [4], [5]. But neither these rules nor the aspect ratio give any hint on how to improve on the integrity problems mentioned above.

As a possible solution we take a look at the penetrator stress. This has already been proposed in an earlier contribution [6], and we will briefly recall the main results for better comprehension of the following. In order to get a simple but generally valid description, we assume a working hypothesis that considers the penetrator to be a bending rod with a uniform transverse load. This leads to a more universally applicable insight and also – as we will show – to a simple transformation rule or scaling parameter for penetrators of different shapes (in the sense of 'not ***L/D***-scaled' rods).

Then, for the general description of a bending rod it does not really matter which special bending case we look at. We consider the bending rod to be a prismatic body of circular cross-section (Figure 5). The rod of diameter D and length L is supported at both ends and carries a uniform transverse load. The moment thus induced results in a bending of the rod with a radius r. The quantity ε denotes the maximum deflection.

For the load condition of the bending column as depicted in Figure 5 the ruling equations are those of bending moment $M = q \cdot L^2/8$, moment of resistance $W = I/(D/2)$ and areal moment of inertia $I = \pi \cdot D^4/64$, see [6], [7].

In the case of penetrator acceleration and target interaction it is very likely that the acting bending forces are mass forces being induced by the rod proper weight, i.e. we assume that the uniform transverse load is caused by lateral acceleration. The total load is then calculated by Newton's Law as $F = \pi/4 \cdot D^2 \cdot L \cdot \rho \cdot a_q$. Herein the transverse acce-

leration a_q is defined as a multiple of the normal acceleration g due to gravity, i.e. $a_q = n \cdot g$. With $q = F/L$ the load per unit length on the rod is calculated to be $q = \pi/4 \cdot D^2 \cdot \rho \cdot a_q$.

Now, from the general equation for the *bending stress* in the case of a rod under uniform transverse load the following expression can be derived:

$$\sigma_B = \frac{q \cdot L^2}{8 \cdot W} = \rho \cdot a_q \cdot \left(\frac{L}{D} \cdot L \right) .$$

The maximum *pitch of deflection sag* is written as

$$\varepsilon = \frac{5}{384} \cdot \frac{q \cdot L^4}{E \cdot I} = \frac{5}{24} \cdot \frac{\rho \cdot a_q}{E} \cdot \left(\frac{L}{D} \cdot L \right)^2 ,$$

and the *curvature* of the transversely loaded rod is given by

$$k = \frac{M}{E \cdot I} = 2 \cdot \frac{\rho \cdot a_q}{E} \cdot \left(\frac{L}{D} \right)^2 .$$

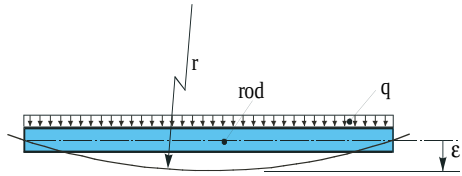

D	diameter
L	length
E	Young's modulus
ρ	density
q	uniform load
ε	deflection
r	bending radius
k=1/r	curvature

Figure 5. Cylindrical rod, uniform bending load.

PENETRATORS OF CONSTANT BENDING STRESS

A better insight can be achieved if we only compare homogeneous rods made of the same material. Then the factors containing ρ, E and a_q remain constant. If the recurring expressions are named as $(L/D) \cdot L = f_L$ and $(L/D) = \lambda$, respectively, this results in the following direct proportions for

Bending stress:

$$\sigma_B \sim a_q \cdot \left(\frac{L}{D} \cdot L \right) = a_q \cdot \left(\frac{L}{D} \right)^2 \cdot D = a_q \cdot f_L$$

Maximum deflection:

$$\varepsilon \sim a_q \cdot \left(\frac{L}{D} \cdot L \right)^2 = a_q \cdot \left(\frac{L}{D} \right)^4 \cdot D^2 = a_q \cdot f_L^2 .$$

Curvature:

$$k \sim a_q \cdot \left(\frac{L}{D} \right)^2 = a_q \cdot \lambda^2 .$$

These equations have interesting consequences: If we assume *identical transverse accelerations* for the rods the dimensions of which are chosen with different diameters and lengths in such a way that

$$f_L = (L/D) \cdot L = (L/D)^2 \cdot D = const.,$$

then for penetrators of equal material the following conclusions can be drawn: The rods show identical maximum bending stress and identical maximum deflection. This is of course quite an interesting aspect as far as design and construction of long-rod penetrators are concerned.

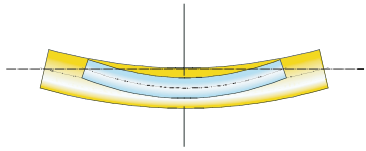

Figure 6: Sketch of bended rods; f_L = *const.*; diameter ratio: 2:1.

Figure 6 gives an impression of the bending behaviour of two rods designed according to the f_L-rule. At a diameter ratio of 2 the length only increases by the factor of $\sqrt{2}$; and we achieve identical deflections.

If we take the criterion for geometrically similar rods, i.e.

$$\lambda = L / D = const.$$

as a construction rule, then these penetrators show identical curvature of bending when charged by forces due to identcal transverse accelerations (see figure 7).

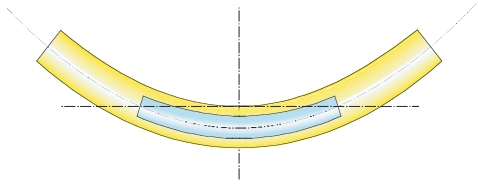

Figure 7: Sketch of bended rods; l=const.; diameter ratio: 2:1; the small rod is identical to the one in Figure 6.

There are some interesting consequences of the above mentioned equations.

- Generally speaking, for rods under lateral acceleration the bending stress is a square function of the length and inversely proportional to the diameter. The deflection is proportional to the forth power of the length and inversely proportional to the square of the diameter.
- For rods with constant aspect ratios the bending stress turns out to be directly proportional to the diameter, whereas the deflection is a square function of the diameter.
- In any case the curvature shows a square dependency on the aspect ratio.
- The parameter f_L is an indicator for the sensitivity and the reaction of bending rods to lateral load. Increasing values of f_L mean increasing bending stresses and increasing deflections of the rod.

EVALUATION OF EXPERIMENTS

The theoretical results described above can now be applied to experiments performed with long rod penetrators. As no information was obtainable on acceleration data of the rods and therefore a straight forward calculation is not feasible, we suppose to demonstrate the inverse procedure: Starting from the visible experimental results, as to say the

deflection of the bars, we shall now evaluate the acceleration forces necessary to cause that deflection and also the corresponding bending stresses.

Figure 8 (B-21022 / X-Ray: GR.FA.26)

Figure 9 (B-21006 / X-Ray: GR.FA.26)

Figure 10 (B-21015 / X-Ray: GR.FA.26)

Figure 8, 9 and 10: Long-rod penetrators after target interaction (pictures are not in scale).

Projectiles after Target Contact (Full-Scale Experiments)

The Figures 8, 9 and 10 show X-Ray photographs from 4 real-scale experiments with penetrators of different lengths, diameters and aspect ratios (λ=21.6, 22.1 and 30) after having penetrated a target plate at an angle of 60°NATO. The maximum deflection was measured from the photographs and then converted according to the angle between bending plane and projection plane (measured by yaw cards). Table 1 gives the main penetrator dimensions, the value of maximum deflection as well as the corresponding calculated data for the transverse acceleration and the induced bending stress, respectively.

It can be noticed, that the bending stress data for these experiments do not differ very much despite of the remarkable difference in the lateral acceleration rate. This is mainly due to the diameter difference causing an increase in mass per unit length of some 60% while comparing 1st to 2nd example. Also the total bending force (not listed) for case 2 is still higher by about 25% despite of the acceleration ratio of (1.34:1).

Table 1: Acceleration and Stress as calculated from experimental data

	(name)	D	L	λ	f_L	ε	a_q	σ_B
figure	*(unit)*	*mm*	*mm*	*1*	*m*	*mm*	*m/s²*	*N/mm²*
8	21022	24	530	22.1	11.7	13.1	9155	1886
9	21006	31	670	21.6	14.5	14.9	6815	1737
10	21015	22	660	30.0	19.8	19.3	4695	1636

The stress level is relatively high if we take the dynamic strength of the rod material to be 1350 N/mm² (Figure 8, 9) and 1500 N/mm² (Figure 10). As there is no indication of fracture two possible explanations can be given: Increase of dynamic strength due to high strain rates or onset of plastic deformation. In the latter case the calculated stress data are no longer realistic values but only indicators for exceeding the elastic region and the dynamic strength.

As the accelerations are all different, the parameter f_L can of course only serve as an indicator for the bending properties of the particular rod and not anymore as a parameter for equal stress rods. In that respect the simultaneous increase of the parameter f_L and the deflection ε is accidental as well as the increase of stress with acceleration. But as a matter of principle the interdependencies according to the basic equations derived above do hold.

Projectiles after Launch (Model-Scale and Full-Scale Experiments)

Figure 2a and Figure 2b clearly demonstrate the bending of long-rod projectiles with an aspect ratio of 40 travelling at velocities of about 1750 m/s. The X-Ray pictures were taken shortly after acceleration with a 40 mm gun at 1.5 m and 20 m downrange the muzzle. Experimental results and calculated data are listed in Table 2 (wherein D' stands for the diameter of a rod with equal mass). In contrast to the data in Table 1 and as a consequence of identical rods we now find bending stresses to be proportional to accelerations. The penetrators show bending stresses at medium to high level but still below the dynamic strength of the rod material (1200 N/mm²).

Table 2: Acceleration and Stress as calculated from experimental data

	(name)	D	L	λ	f_L	ε	a_q	σ_B
figure	*(unit)*	*mm*	*mm*	*1*	*m*	*mm*	m/s^2	N/mm^2
2a	p06.7C8	5.56	224	40.3	9.0	2.42	4720	750
2b	p05.7C8					3.41	6650	1057
3	Pfeil-GE	26.2	950	36.3	34.5	11.0	1480	897

The full-scale experiment (Figure 3) shows an interesting result: The extremely long projectile has a maximum deflection of 11 mm which is compared to the scaled rods about proportional to the length. Yet the acceleration is much less (as might be expected comparing the longitudinal accelerations of different calibre guns), whereas the bending stresses match quite well. The reasons for this have already been explained earlier, and one should refer to the nearly equal values of aspect ratios but strongly differing bending parameters f_L.

At a first glance it is nevertheless astonishing to recognize that the rods may suffer from bending stresses at this level when being accelerated in longitudinal direction. Two reasons can be given: Either we assume – as discussed and calculated above – transverse accelerations (which turned out to be in the order of about 1% of the longitudinal acceleration), or we admit longitudinal acceleration forces not aligned with or attacking out of axis. As a matter of fact bending stresses become equal to axial stresses if the axial force attacks at a measure of 1/8 of the diameter out of centre (i.e. 0.7 mm in the case of Figure 2). Because of the superposition of the forces these effects can be crucial to the integrity of the projectile.

Transverse Acceleration Experiments

Evaluation of experimental results only from deflection data bear some uncertainties especially concerning load and support conditions. To overcome this difficulties we performed special acceleration experiments where load and acceleration conditions could perfectly be controlled. In contrast to the above mentioned experiments the rods were now subjected to a transverse acceleration exactly as postulated by theory. This was done by the aid of a special (electromagnetic) "pancake" coil accelerator where the payload consisted of a conductor disc, bar support and test bar, see Figure 11. The bar support was designed to hold rods of different dimensions and masses – the total payload mass being kept constant in order to guarantee constant acceleration.

Starting from a rod with $D=3$ *mm* and $L=30$ *mm* ($\lambda=10$; $f_L=0.3$) the two other rods were designed with twice the diameter and according to the $f_L=const.$ and $\lambda=const.$ rule, see Table 3 and Figure 12. The acceleration was chosen to cause a subcritical bending stress for the constant stress rods, but should provoke rupture for the rod with equal aspect ratio. Figures 13 to 15 show the X-Ray pictures taken from the experiments performed with identical accelerations. It is obvious that the two rods with a diameter of 6 mm behave differently: The rod with $f_L=0.3$ shows exactly the same deformation and shape as the rod with 3 mm diameter, whereas the rod with $\lambda=10$ breaks into pieces because of the bending stresses differing by the factor of 2 (compare Table 3).

Table 3: Transverse acceleration experiments of rods with diameter ratio 1:2

	(name)	D	L	λ	f_L	a_q	σ_B
figure	*(unit)*	*mm*	*mm*	*1*	*m*	*m/s²*	*N/mm²*
13	S-RX.3	3	30.0	10.0	0.3	181000	960
15	S-RX.7	6	42.5	7.08			
14	S-RX.8		60.0	10.0	0.6		1920

Thus the theoretical considerations could be proved by experiment. Furthermore it becomes evident that full-scale penetrators are much more likely to break of bending stresses than model-scale rods of equal L/D-ratio, taken that the stresses are caused by identical lateral accelerations.

FINAL REMARKS

From a relatively simple hypothesis on the load of bending bars by mass forces we could establish a parameter which defines rods of constant bending stresses. Generally valid rules for rods under lateral accelerations were discussed and proven by some properly designed experiments. The parameter is not only useful for designing long-rod penetrators but also – as could be shown – it can be taken as a tool to calculate accelerations and stresses the penetrator has suffered. Of course one should not expect a very high accuracy as there are quite a number of parameters which can not be defined very precisely, as for example load and support conditions for the case in consideration. Nevertheless it could be shown that the procedure gives a more or less accurate estimate of the penetrator

status after acceleration or even penetration of a target as far as maximum bending stresses or elastic and plastic regimes are concerned.

Considering the equations derived above, it would be of some interest to compare model-scale and full-scale experiments with corresponding penetrator data to each other. If the lateral acceleration of the rod could be measured while penetrating a (possibly mobile) target this would give a very useful straight forward explanation of penetrator success or failure and hence some hints for an optimal penetrator design with regard to lateral forces and structural integrity.

REFERENCES

1. Lehr, H. F., Wollmann, E., Koerber G. "Experiments with jacketed rods of high fineness ratio". *Int. J. of Impact Engng.*, 1995; 17: 517–526.
2. Lanz, W., Lehr, H. F. "Craters caused by jacketed heavy metal projectiles of very high aspect ratios impacting steel targets". *Proc. 16th Int. Symp. on Ballistics*, San Franzisco, CA, USA, 1996.
3. Cranz, C. Lehrbuch der Ballistik. Dritter Band, Springer Verlag, Berlin, 1927.
4. Weihrauch, G., Lehr, H. F., Wollmann, E. "Anwendung klassischer Panzerformeln auf Wuchtgeschosse". In: *Handbuch Munitionsbewertung*, BWB WM VI 2, Koblenz, Germany, 1979.
5. Lehr, H. F., Weihrauch, G. "Evaluation of perforation power of kinetic energy projectiles by Martel's hypothesis". *Proc. 5th Int. Symp. on Ballistics*, Toulouse, France, 1980.
6. Lehr, H. F., Wollmann, E. "On a new shape parameter and the conception of rod penetrators considering strength criteria". *Proc. 18th Int. Symp. on Ballistics*, San Antonio, TX, USA, 1999.
7. Dubbel, 16. Auflage, Springer-Verlag, Berlin, Heidelberg, New York, London, Paris, Tokyo, 1987.

Figure 1: Long-rod projectile, cal. 40 mm, L/D=40.

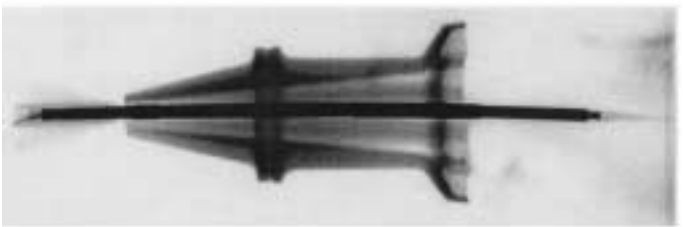

1,5 m

G 176 A, 7C7. 39 20 m Vo 1790 m/s

Figure 2a: Long-rod projectile, sabot separation; free flight.

G 176 A, 7C7. 38 20 m Vo 1710 m/s

Figure 2b: Long-rod projectile in free flight showing severe bending.

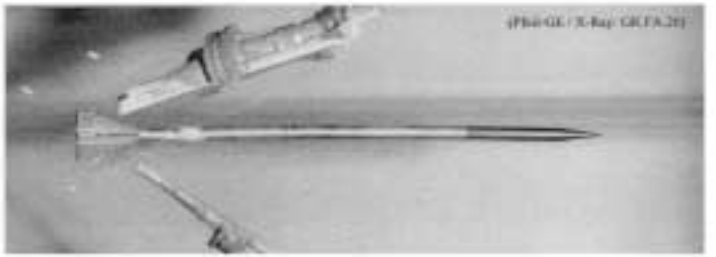

Figure 3: Full scale long-rod projectile, sabot separation, bending.

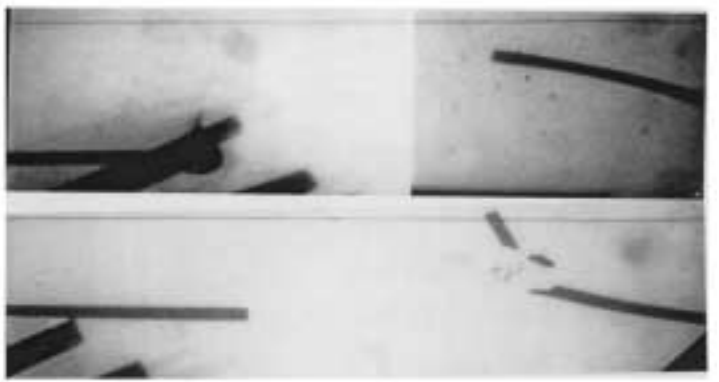

Figure 4: Bending effects (above) and fracture (below) affecting long rods caused by interaction with moving plate.

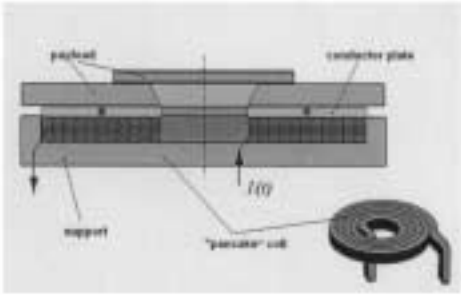

Figure 11: “Pancake” coil accelerator.

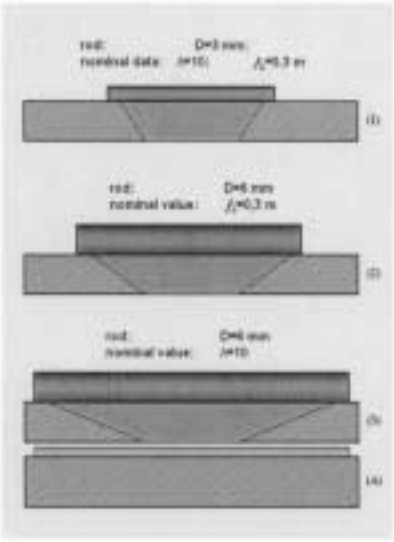

Figure 12: “Pancake” coil acceleraor (A); three different payloads.

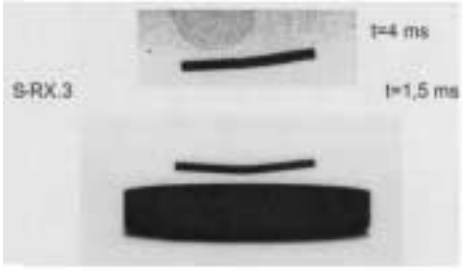

Figure 13: Acceleration of a rod *D=3 mm, L/D=10, f_L=0,3 (see Table 3).*

t=4,7 ms

S-RX.8

t=1,5 ms

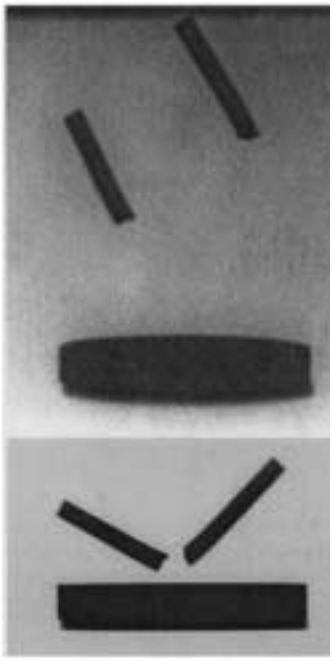

Figure 14: Acceleration of a rod *D=6 mm, L/D=10 (see Table 3).*

t=4,7 ms

S-RX.7

t=1,5 ms

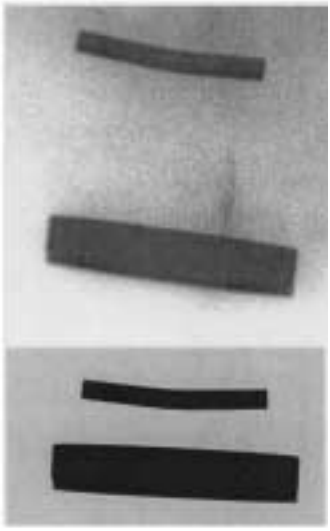

Figure 15: Acceleration of a rod *D=6 mm, f_L= 0,3 (see Table 3).*